

Supplemental methods: Algorithms Used in the Analysis section

1. Detection of Phase Singularities

A phase singularity (PS), which forms the tip of a reentrant wave, was defined on the basis of a transform of membrane potential distribution into phase as described earlier.³ The algorithm used to detect PSs was based on the algorithm proposed by Zou et. al.⁴ Since the tip of the reentrant spiral wave is surrounded by tissue in all phases, from activation to recovery, PSs can be identified as area containing all phases of the action potential simultaneously.

2. Computation of Lifespan of Phase Singularities

To investigate the dynamics of PSs propagation, they were tracked in time and space as follows. The distance was calculated between all PSs detected at simulation time $t + 1$ ms and all PSs detected at simulation time t . If the minimum distance was less than 1mm, the two PSs were assigned the same ID. If for a PS the minimum distance was larger than 1mm, the PS was considered as an independent PS and was assigned a new ID. By choosing 1mm as a threshold, it was assumed that a PS cannot move faster than 1m/s.³

3. Detection of Breakthroughs

A breakthrough (BT) is a wave that appears in one layer and cannot be related to the propagation of other waves in the same layer. To detect BTs, areas containing connection points were studied per each 1ms. If a wave appeared at a connection point, this wave was followed for 2ms as a candidate breakthrough. If the breakthrough candidate increased in size within 2ms, it was labeled as a breakthrough. The moment of breakthrough appearance and the location were stored for further analysis.

4. Breakthrough Propagation Tracking

Dynamics of breakthrough propagation was explored using the wave chain tracking algorithm described in our previous work.³ In this algorithm, labeled wave(s) as well as breakthrough(s)

were tracked through time and space. Lifespan of a breakthrough was defined as the time duration between breakthrough appearance and either extinction or fusion with a bigger wave. Breakthroughs were tracked in time by comparing AF patterns each 1ms, similar to the approach reported by Ten Tusscher et al.⁵ and Clayton et al.⁶

5. Detection of Fibrillation Waves

A wave was defined as a contiguous area in which all segments have trans-membrane voltages above the excitation threshold of -60mV. Number of waves was calculated each 1ms of simulation time.

6. Computation of Wave Front Lifespan

The propagation of fibrillation waves in our model was analyzed by tracking wave fronts through time and space. Wave fronts were detected using maximum positive slope in trans-membrane potentials.

The temporal dynamics of wave fronts can be described by three events:

- Extinction: the disappearance of a wave fronts, because it hits a boundary or runs into unexcitable tissue;
- New wave front generation: appearance of a new wave front because a wave front breaks up into two or more wave fronts;
- Fusion: the merging of two or more wave fronts into one wave front as they collide with each other.

Wave fronts were tracked in time by comparing AF wave front patterns in each 1ms, similar to the approach reported by Ten Tusscher et al.⁵ and Clayton et al.⁷ For all wave fronts found in each layer at simulation time t , overlap (amount of segments) is computed with all wave fronts found in that layer at simulation time $t + 1$. If a wave front in one layer at simulation time t does

not have overlap with any wave fronts in that layer at simulation time $t + 1$, it means that the wave front was extinguished. If a wave front at simulation time $t + 1$ has overlap with two or more wave fronts at simulation time t , fusion occurred. If a wave front at simulation time t has overlap with two or more wave fronts at simulation time $t + 1$, wave break occurred and a new wave was generated. Finally, if a wave appeared at simulation time $t + 1$ and has no overlap with any wave fronts at simulation time t , breakthrough occurred also resulting in a new wave front.

Identification numbers (IDs) were assigned as follows. At simulation time $t = 1$, all wave fronts in both layers were detected and obtained an ID. If a wave was extinguished, the ID of that wave front was not to be used again. If, because of wave break, one or more new wave fronts were generated, the size of all new wave fronts was calculated. The largest one kept the ID of the mother wave fronts, while the remaining wave fronts obtained new IDs. If fusion occurred, the size of all wave fronts that merged was calculated and the merged wave obtained the ID of the largest one. Breakthrough wave fronts always obtained a new ID.

7. AF Cycle Length (AFCL)

AFCL was determined by time differences between two consecutive activation times. A square grid of 40×40 segments was used to reconstruct action potentials (APs). Using these reconstructed APs, activation time has been detected based on most positive slopes with trans-membrane potentials higher than or equal to -60mv .

8. Wave Front Conduction Velocity (WFCV)

Conduction velocity of fibrillation waves was calculated by fitting planes through each detected activation and its neighbors (grid of 15×15 electrodes), including only activations that belonged

to the same fibrillation wave. The local conduction vector was calculated using the orientation of the plane and the reciprocal of the steepness of the plane.⁸

9. Excitable Area (EA)

Total number of segments in both layers with trans-membrane potentials below -60mv is considered as amount of excitable area calculation.

2-3-10. Calculation of dyssynchrony

Dyssynchrony was defined as the percentage of segments that were excited (membrane potential above -60 mV), while the opposing segment was not excited (membrane potential below -60mv), i.e.

$$\text{Dyssynchrony} = \frac{\text{number of cells activated in one layer}}{\text{total number of cells}} \times 100\% \quad (2)$$

Note that this formula does not take the phase of action potential (AP) into account.

To estimate the highest degree of dyssynchrony in each simulation, the average amount of dyssynchrony was calculated during the first 50ms after adding the extra connection points.

11. Endo-epicardial dissociation

Endo-epicardial dissociation was calculated by fitting a two component Gaussian function to histograms of endo-epicardial activation time differences as described previously.⁹ This calculation was performed in addition to dyssynchrony to allow for direct comparison of our simulation results with previously published experimental data.⁹

12. AF Survival Rate

Percentage of simulations in which AF episodes were terminated before 6000ms divided to all number of simulations in each group (8 simulations) were defined as survival rate.

13. Numerical methods and implementation

The model used for the present simulation study was based on our previously published bi-domain model.¹⁵ The mono-domain equation was solved assuming no-flux boundary conditions using an explicit numerical scheme with time steps of 0.01ms as previously described.¹⁶ Gating variables and intracellular ion concentrations were updated with time steps of 0.01ms during the action potential upstroke and with time steps of 0.1ms otherwise.¹⁷ Gating variables were integrated using the Rush-Larsen method.^{13, 18} The model was implemented in C++ and executed on a normal PC with Intel i7 processor and 6GB memory. It took 72 hours to simulate an AF episode of 6s. Up to six simulations could run simultaneously on the multi-core processor without an increase in computation time.

14. Statistical analysis

All statistical analyses were performed using STATA 12.1 (StataCorp, 2009).

Statistical tests were performed to compare the 6 groups of simulations (6, 12, 24, 48, 96, and 100% connectivity), two groups of stable AF and non-stable AF, and parameters associations with AF duration.

The average number of waves, phase singularities, breakthroughs, dyssynchrony percentage, and breakthrough lifespan during whole simulation period were calculated for each individual simulation. The results of the 6 groups were compared using one-way ANOVA with a Bonferroni correction.

For comparing two groups of sustained AF and non-sustained AF, all results were tested for normal distribution. Normally distributed parameters were compared with a parametric t-test. In all other cases a non-parametric Mann–Whitney–Wilcoxon test was used.

Multilevel logistic regression analysis was used for investigation of parameter association with atrial fibrillation stability by dividing simulations in sustained and non-sustained AF.

Supplemental data:

1. Simulations with heterogeneous distribution of connections

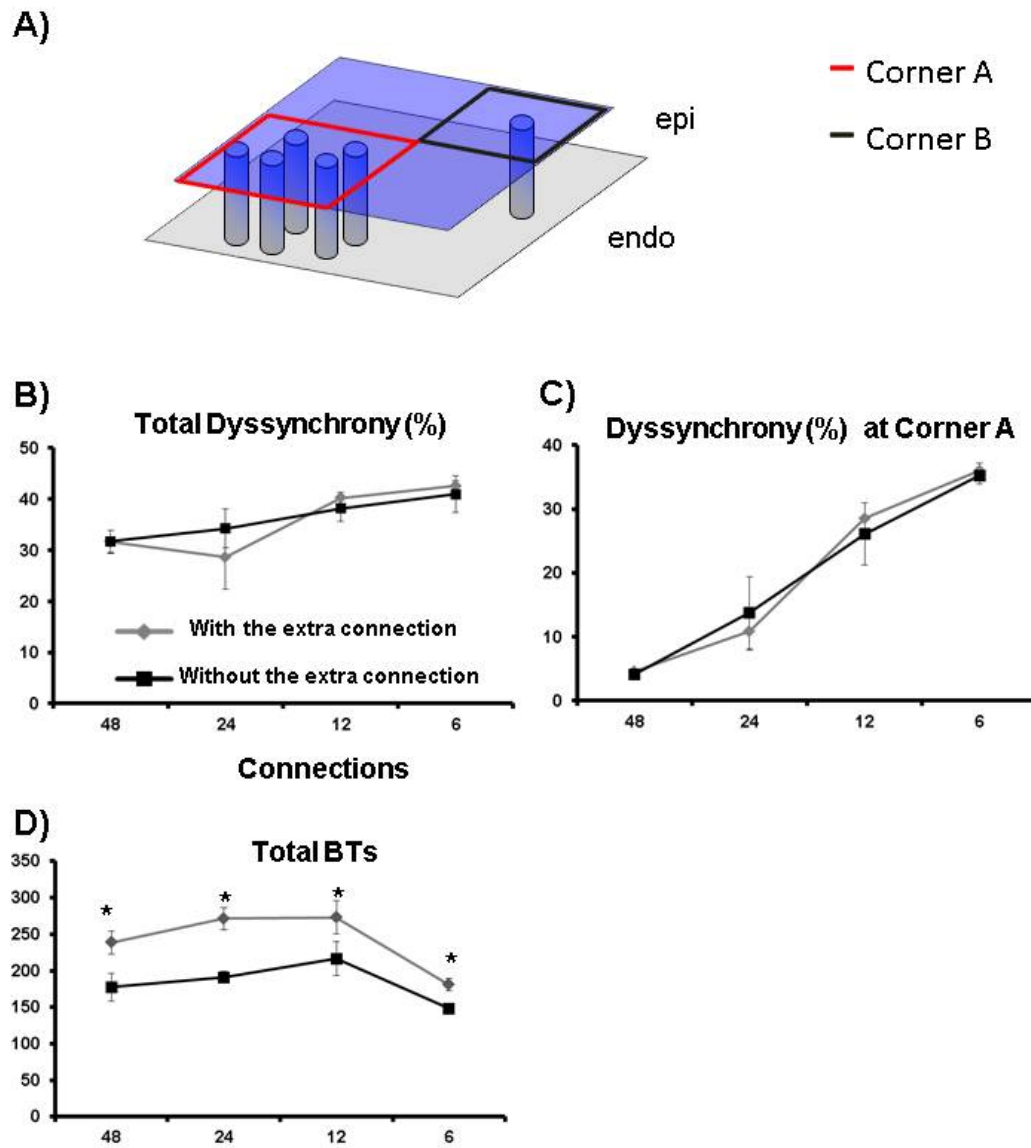
These simulations were performed as below:

1. All simulations performed in step 1 (see method section) were taken as starting point.
2. For the different numbers of connections (6, 12, 24, and 48), the connections were randomly distributed within one corner of the simulated tissue (quadrant A, see extra figure 1A).
3. All simulations in step 2 were continued either with an extra connection at the opposite corner (quadrant B, see extra figure 1A) or without the extra connection.

We did not increase the number of connections to more than 48 connections, because a higher number of connections would not fit within quadrant A.

As illustrated in extra figure 1B, we calculated the number of breakthroughs and dyssynchrony for each group. The degree of dyssynchrony was calculated in either the whole simulated tissue (total dyssynchrony) or only at the quadrant A. Dyssynchrony calculated in the corner A was strongly dependent on the number of connections and it was increased by a reduction in number of connections. Adding the extra connection in quadrant B had no effect on the level of total dyssynchrony and on the dyssynchrony at quadrant A. Interestingly, a decrease in the number of connections in quadrant A also had no effect on total dyssynchrony. Adding the extra connection significantly increased the occurrence of BTs. In both groups, adding or removing connections in

quadrant A had no significant effect on the number of BTs. Therefore, the distribution of connections is an important factor for the number of BTs modulation, and connections that are very closely apposed essentially act as a single connection.



Extra figure 1. **Heterogeneous distribution of connections.** A) Model structure with a clustered distribution of connections. B) Calculated dyssynchrony in the entire simulation area. C). Calculated dyssynchrony within quadrant A. D) Total BT occurrence in simulation without and with an extra connection in quadrant B.

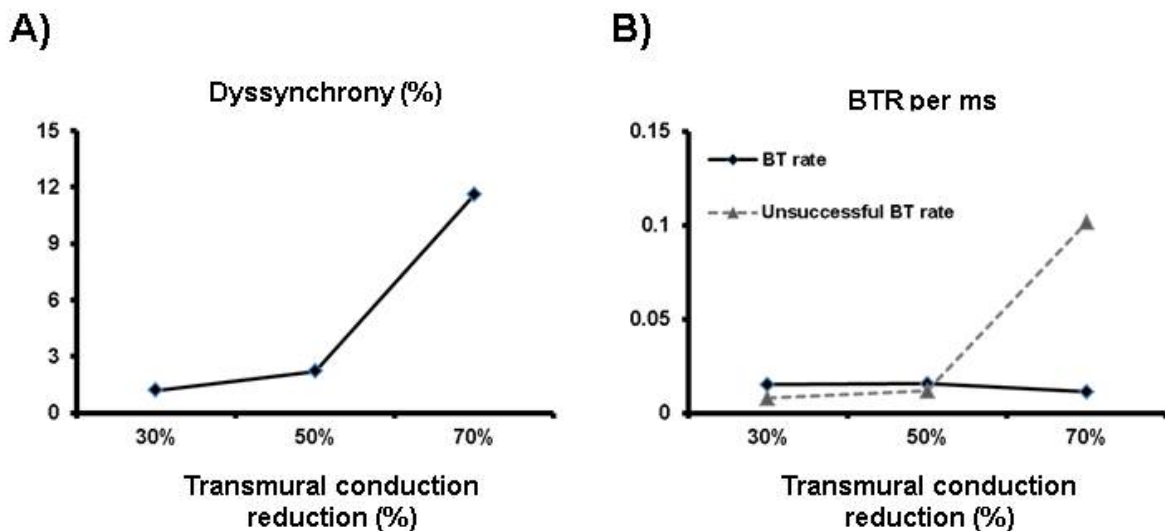
2. Simulations with a reduced conductivity of end-epicardial connections

Simulations with 96 connections were taken. In all segments that were located in endo-epicardial connection area, we simulated different degrees of reduction in both longitudinal and transversal conductivities. A reduction larger than 70% led to complete conduction block and therefore those simulations were not included in the results.

As illustrated in extra figure 2A, a decrease in conductivity increased dyssynchrony of electrical activity between the two layers. A reduction in transmural conductivity to 30% and 50% only slightly increased the dyssynchrony of electrical activity. A reduction of the transmural conductivities to 70% did have a marked impact on the electrical activity dyssynchrony.

As shown in extra figure 2B, the BTR did not differ significantly between the varying degrees of transmural conductivity. Interestingly, the rate of unsuccessful BTs (BTs that did not successfully propagate) in case of a 70% reduction of transmural conductivity increased dramatically. This means that with a 70% reduction in transmural conductivity, the increase in dyssynchrony did lead to more potential BTs, but that because of the reduced transmural conductivity, most of them did not propagate.

Figure 2



Extra figure 2. **Reduced conductivity of end-epicardial connections.** Effect of the reduction of transmurality conductivity on A) degree of dyssynchrony and B) the rate of successful and unsuccessful breakthroughs.

Reference:

1. Verheule S, Tuyls E, Gharaviri A, Hulsmans S, van Hunnik A, Kuiper M, et al. Loss of continuity in the thin epicardial layer because of endomysial fibrosis increases the complexity of atrial fibrillatory conduction. *Circ Arrhythm Electrophysiol* Feb 2013;6:202-211.
2. Schneider CA, Rasband WS, Eliceiri KW. NIH Image to ImageJ: 25 years of image analysis. *Nature methods* Jul 2012;9:671-675.
3. Gharaviri A, Verheule S, Eckstein J, Potse M, Kuipers N, Schotten U. A computer model of endo-epicardial electrical dissociation and transmurality conduction during atrial fibrillation. *Europace* Nov 2012;14 Suppl 5:v10-v16.
4. Zou R, Kneller J, Leon LJ, Nattel S. Development of a computer algorithm for the detection of phase singularities and initial application to analyze simulations of atrial fibrillation. *Chaos* Sep 2002;12:764-778.
5. Ten Tusscher KH, Hren R, Panfilov AV. Organization of ventricular fibrillation in the human heart. *Circ Res* Jun 22 2007;100:e87-101.
6. Clayton RH, Holden AV. Dynamics and interaction of filaments in a computational model of re-entrant ventricular fibrillation. *Phys Med Biol* May 21 2002;47:1777-1792.
7. Clayton RH, Holden AV. A method to quantify the dynamics and complexity of re-entry in computational models of ventricular fibrillation. *Phys Med Biol* Jan 21 2002;47:225-238.

8. Houben RP, de Groot NM, Smeets JL, Becker AE, Lindemans FW, Allessie MA. S-wave predominance of epicardial electrograms during atrial fibrillation in humans: indirect evidence for a role of the thin subepicardial layer. *Heart Rhythm* Dec 2004;1:639-647.
9. Eckstein J, Maesen B, Linz D, Zeemering S, van Hunnik A, Verheule S, et al. Time course and mechanisms of endo-epicardial electrical dissociation during atrial fibrillation in the goat. *Cardiovasc Res* Mar 1 2011;89:816-824.

Movie Legends

Movie1 . 6 Connections. An example of dual layer AF simulations with 6 connections.

Movie2 . 12 Connections. An example of dual layer AF simulations with 12 connections.

Movie3 . 24 Connections. An example of dual layer AF simulations with 24 connections.

Movie4 . 48 Connections. An example of dual layer AF simulations with 48 connections.

Movie5 . 96 Connections. An example of dual layer AF simulations with 96 connections.

Movie6 . 100% Connectivity. An example of dual layer AF simulations with 100% connectivity.